




Hall effect in a two-dimensional disordered Lorentz gasBenjamin Sanvee,¹ Jakob Schluck ,^{2,3} Mihai Cerchez,² Dominique Mailly,⁴ Hans W. Schumacher,⁵ Klaus Pierz ,⁵ Thomas Heinzl,² and Jürgen Horbach ¹¹*Institut für Theoretische Physik II, Heinrich-Heine-Universität Düsseldorf, Universitätsstraße 1, 40225 Düsseldorf, Germany*²*Institut für Experimentelle Physik der kondensierten Materie, Heinrich-Heine-Universität Düsseldorf, Universitätsstraße 1, 40225 Düsseldorf, Germany*³*II. Physikalisches Institut, Universität zu Köln, Zùlpicher Str. 77, 50937 Köln, Germany*⁴*Université Paris-Saclay, CNRS, Centre de Nanosciences et de Nanotechnologies, 91120 Palaiseau, France*⁵*Physikalisch-Technische Bundesanstalt, Bundesallee 100, 38116 Braunschweig, Germany*

(Received 3 April 2023; revised 23 June 2023; accepted 23 June 2023; published 5 July 2023)

Using a combination of experiment and simulation, we study the magnetotransport in a two-dimensional disordered Lorentz gas with circular obstacles. Our focus is on the investigation of the Hall effect at obstacle densities beyond the low-density limit. However, as a reference, we also consider very low obstacle densities. Here, the magnetotransport properties, as obtained from the simulation and the experiment of a pristine sample, can be well described in terms of the Drude-Boltzmann model. For intermediate and high obstacle density, only for very low magnetic fields B , we find a linear dependence of the Hall resistance ϱ_{xy} on B , albeit *with a Hall coefficient that does not reflect properly the carrier density*. At larger magnetic fields but still below the onset of the Landau quantization as well as the magnetic-field-induced conductor-to-insulator transition, striking nonlinearities of $\varrho_{xy}(B)$ due to classical memory effects are observed. Moreover, the scattering time obtained within the Drude-Boltzmann model develops into a phenomenological parameter that decreases with increasing magnetic field.

DOI: [10.1103/PhysRevB.108.035301](https://doi.org/10.1103/PhysRevB.108.035301)**I. INTRODUCTION**

Lorentz gases can be seen as a paradigm for the study of transport phenomena in heterogeneous media [1,2]. A simple disordered version of a two-dimensional (2D) Lorentz gas consists of a fluid of noninteracting tracer particles that is exposed to a random arrangement of circular obstacles. An experimental realization of such a system can be achieved via a two-dimensional electron gas (2DEG) with lithographically imprinted obstacle structures. In particular, such a 2DEG in Ga[Al]As semiconductor heterostructures often provides electrons with a high mobility that one can consider to a good approximation as quasiclassical noninteracting fermions. Experimental realizations of Lorentz gases with such 2DEGs and circular obstacles with a radius of the order of a micrometer can be well modelled in terms of classical molecular dynamics (MD) simulations. In this paper, we use a combination of experiment and MD simulation to elucidate the magnetotransport in a 2D disordered Lorentz gas, with a special focus on the Hall effect.

Since its discovery [3], the Hall effect, i.e., the buildup of a transverse voltage in conductors exposed to a perpendicular magnetic field B , has developed into a whole family of phenomena, like the quantized Hall effects [4,5], the spin Hall effect or anomalous Hall effects in topological insulators. Its relevance for scientific and technological progress can hardly be overestimated. For example, the integer quantum Hall effect is used as resistance standard, and the study of the fractional quantum Hall effect has triggered the concept of composite fermions [6]. Hall sensors are omnipresent to

detect magnetic fields, and carrier densities in metals and semiconductors are routinely determined from the Hall resistance as a function of B . Its slope is usually constant with a high robustness in nonferromagnetic materials. Corrections of the Drude conductivity by electron-electron interactions [7,8] have been reported in samples of relatively low electron mobility [9–11]. They cause a temperature-dependent Hall slope without textures as a function of the magnetic field. Weak localization, the most prominent quantum correction at small magnetic fields, does not influence the Hall slope in the single particle picture [7,11]. At low mobilities below $\approx 1 \text{ m}^2/\text{Vs}$, the interplay of interactions and weak localization can cause a B dependence of the Hall slope [12]. Furthermore, in the absence of interactions, the Hall slope is not expected to show a temperature dependence for constant carrier densities [13].

Some mechanisms causing nonlinearities, however, are known, such as magnetic-field induced electron transfers between the free electron gas and a nearby doping layer [14], interactions close to the metal-insulator transition [15,16], edge and impurity scattering in ballistic Hall crosses [17–19], and localized spins [20]. A recently discovered type of nonlinear Hall effect is the quadratic dependence of the Hall voltage on the driving current, which originates from a broken inversion symmetry and is suited to study topological aspects of quantum phases [21]. Here, we report the detection of nonlinearities in the Hall effect in a 2D Lorentz gas that originate from classical memory effects and render the conventional carrier density determination from a Hall analysis inaccurate for samples containing such obstacles to a

substantial density. The effects reported here thus have a distinctly different character than the negative Hall resistance reported for periodic arrays of obstacles, where the magnetic-field dependent guidance of the electrons through the array plays an important role [22]. Furthermore, the reported nonlinearities in the Hall slope, which have been explained in terms of rings of low, temperature-dependent resistivity around each element of a periodic antidot lattice [23] have a very different character. It should be noted that the physics of 2D Lorentz gases discussed here is substantially different from that of *antidot lattices* [24–26], where the arrangement of the obstacles is periodic rather than random, leading to a characteristic mixed phase space where regular islands are embedded in a chaotic sea of motion, which manifests itself via classical commensurability resonances in the magnetoresistance. This phenomenology is strongly suppressed by relatively small deviations from a perfect periodicity of the obstacles [27] or by additional disorder [28] and thus absent in Lorentz gases. The obstacles present in our samples are in the classical regime, and one can neglect a weak localization correction, which has been reported to generate nonlinearities in the Hall effect in some inhomogeneous two-dimensional electron systems [29]. In this paper, we also study the magnetotransport of Lorentz gases in the regime of very low densities. Since the size of our obstacles is larger than the Fermi wavelength, our samples are in the classical regime, in the sense that the obstacles do not modify the weak localization [30]. Both the experimental and the simulation data indicate for this regime that the Drude-Boltzmann (DB) theory, based on a linear Boltzmann equation, provides a quantitatively accurate description of magnetotransport properties and the Hall effect over the entire range of magnetic fields. This finding challenges a theory of Bobylev *et al.* [2,31,32], based on a generalized Boltzmann equation. Below, we also discuss a theoretical approach of Dmitriev *et al.* [33,34] where corrections to the Hall coefficient according to DB theory are calculated via an *ad hoc* modification of the Boltzmann equation.

In the next Sec. II, we highlight some specific properties of the Drude and the (generalized) Boltzmann model, which are relevant for the description of Lorentz gases. Section III introduces the considered Lorentz gas model and gives the main details of the simulation. Section IV is devoted to the experimental setup, the measurement techniques, and the determination of the electron density via the Landau quantization of the electronic cyclotron orbits at high magnetic fields. The results on the magnetotransport are presented in Sec. V. Eventually, we summarize and draw conclusions (Sec. VI).

II. THE DRUDE AND (GENERALIZED) BOLTZMANN MODELS IN RELATION TO LORENTZ GASES

The Drude model [35] can be seen as a minimal model for the classical Hall effect. In its two-dimensional version, the electrons are represented as noninteracting tracer particles with charge e in a magnetic field of magnitude B that is oriented perpendicular to the tracer's plane of motion, say in z direction. In the absence of any scatterers, an electron performs a circular motion with cyclotron frequency $\omega_{\text{cy}} = \frac{eB}{m^*}$, with m^* the effective mass of an electron. The surrounding medium by which the electrons are scattered is effectively taken into account in terms of a frictional force $-\frac{m^*}{\tau_{\text{Dr}}} \vec{v}$, with

\vec{v} the velocity of an electron and τ_{Dr} a diffusive time scale that is of the order of the mean free time between two collisions.

A microscopic description that is equivalent to the latter Drude model is provided by the linear Boltzmann equation (LBE) [1]. This is a kinetic equation from which one obtains a quantitative prediction for the diffusive time scale τ_{Dr} (unlike the Drude model where τ_{Dr} is just an “input parameter”). In the framework of the LBE, one considers a two-dimensional Lorentz gas in a square of linear dimension L where a point tracer particle moves through a fixed random arrangement of N overlapping circular obstacles of radius R . The tracer particle is elastically scattered by the obstacles and thus its speed $v_0 = |\vec{v}|$ is a constant of the motion. A control parameter for the transport of the tracer particle is the reduced number density of obstacles, $\rho = \frac{N}{L^2} \pi R^2$. For the case of zero magnetic field B , it has been shown that the LBE becomes exact in the Grad limit [36], i.e., for $\rho \rightarrow 0$ keeping the mean-free path between collisions, $\Lambda = \frac{\pi R}{2\rho}$, constant (this implies $R \rightarrow 0$ and $\rho/R^2 \rightarrow \infty$).

The central quantity to study the magnetotransport in the two-dimensional Lorentz gas is the conductivity matrix σ that can be introduced as follows. Applying a sufficiently small electric field \vec{E} in the plane of motion, i.e., in the xy plane, the resulting steady-state current \vec{j} is given by

$$\vec{j} = \sigma \vec{E}. \quad (1)$$

Here, due to isotropy the diagonal elements of σ are equal, $\sigma_{xx} = \sigma_{yy}$. For the nondiagonal elements, $\sigma_{xy} = -\sigma_{yx}$ holds. The magnetoconductivity σ_{xy} is expected to be nonzero in the presence of a magnetic field.

In the framework of the DB model, the elements of σ can be analytically calculated and one obtains

$$\sigma_{xx} = \sigma_0 \frac{1}{1 + \omega_{\text{cy}}^2 \tau_{\text{Dr}}^2}, \quad (2)$$

$$\sigma_{xy} = \sigma_0 \frac{\omega_{\text{cy}} \tau_{\text{Dr}}}{1 + \omega_{\text{cy}}^2 \tau_{\text{Dr}}^2}, \quad (3)$$

where the conductance of the electron gas at $B = 0$, σ_0 , is given by

$$\sigma_0 = \frac{n_e e^2 \tau_{\text{Dr}}}{m^*}, \quad (4)$$

with n_e the electron density. For the diffusive time scale, the LBE predicts $\tau_{\text{Dr}} = \frac{3}{4} t_0$ with the mean free time $t_0 = \Lambda/v_0 = \frac{\pi R}{2\rho v_0}$. The diffusion constant at $B = 0$ can be expressed as [1]

$$D_0 = \frac{1}{2} v_0^2 \tau_{\text{Dr}} = \frac{3\pi}{16} \frac{v_0 R}{\rho}. \quad (5)$$

Inverting the matrix σ yields the resistance matrix ϱ , with the magnetoresistance ϱ_{xx} and the Hall resistance ϱ_{xy} as two independent elements. According to Eqs. (2) and (3), the magnetoresistance is just the inverse of the zero-magnetic field conductance, $\varrho_{xx} = 1/\sigma_0$, and the Hall resistance follows a simple linear dependence on B ,

$$\varrho_{xy} = R_{\text{DH}} B, \quad (6)$$

where the Drude-Hall coefficient R_{DH} is inversely proportional to the electron density n_e , $R_{\text{DH}} = 1/(n_e e)$.

An essential assumption of the LBE is the “Stosszahlansatz” according to which successive collisions

are uncorrelated and independent of each other. As pointed out by Bobylev *et al.* [2,31,32,37], in the presence of a magnetic field even in the Grad limit memory effects may become important and thus the assumption of uncorrelated collisions might be no longer valid. This is obvious for orbits where the tracer particles move in circles without ever hitting an obstacle. But with a finite probability it is also possible that after the collision with a certain obstacle a tracer particle recollides with the same obstacle. In order to take into account such recollision events, Bobylev *et al.* have proposed a generalized non-Markovian Boltzmann equation that leads to the following modified expressions for σ_{xx} and σ_{xy} :

$$\sigma_{xx} = \sigma_0 \frac{1 - p^2}{1 + \omega_{cy}^2 \tau^2}, \quad (7)$$

$$\sigma_{xy} = \sigma_0 \left[\frac{\omega_{cy} \tau (1 - p^2)}{1 + \omega_{cy}^2 \tau^2} + \frac{p^2}{\omega_{cy} \tau} \right], \quad (8)$$

with $p = \exp(-\frac{\pi}{t_0 \omega_{cy}}) = \exp(-\frac{2\rho v_0 m^*}{eRB})$ and the diffusive time scale τ given by

$$\tau = \frac{t_0}{1 - \frac{1-p^2}{2p^2} \left[\frac{1-p^2}{2p} \ln\left(\frac{1+p}{1-p}\right) - 1 \right]}. \quad (9)$$

The denominator of this expression for τ exhibits a rather weak dependence on the variable p and thus on the magnetic field B . It decreases monotonically from $4/3$ at $p = 0$ ($B = 0$) to 1 in the limit $p \rightarrow \infty$ ($B \rightarrow \infty$). Note that in the limit $p \rightarrow 0$, Eqs. (7) and (8) respectively approach Eqs. (2) and (3), as obtained from the LBE. Below we will compare the predictions for σ_{xx} and σ_{xy} from the LBE and the generalized Boltzmann equation to results from simulation and experiment at very low densities. Another approach that tries to incorporate memory effects into the LBE has been proposed by Dmitriev *et al.* [33,34]. Here, a B -dependent correction to the Drude-Hall coefficient R_{DH} is predicted that becomes stronger towards low magnetic fields. However, below we show that this prediction is not in agreement with the findings from our simulation. Beyond the low-density limit, the transport is strongly affected by memory effects, i.e., correlated collisions with the obstacles that are not taken into account by the low-density theories. For intermediate and high densities, there is only the mode-coupling theory by Götze and Leutheusser [38] that describes the magnetotransport of the Lorentz gas. However, this theory has not been worked out to an extent that systematic comparisons to simulations or experiments would be possible.

In the following, we study the magnetotransport of the disordered two-dimensional Lorentz gas at very low obstacle densities as well as densities that are far beyond the low-density limit. We consider both an experimental realization of the Lorentz gas in terms of a two-dimensional electron gas (2DEG) in a Ga[Al]As semiconductor heterostructure as well as event-driven computer simulations. Our focus is on the understanding of the Hall resistivity ϱ_{xy} ; in particular we extract the Hall coefficient R_H from experiment and simulation and show that it is not possible to obtain reliable estimates for the electron density from the measured values of R_H at intermediate

or large obstacle density. As we shall see, this also requires a thorough study of the longitudinal magnetotransport.

III. LORENTZ GAS MODEL: SIMULATION DETAILS

Classical event-driven simulations [39] are used to study the magnetotransport of a tracer particle with charge $e = 1.0$ and mass $m^* = 1.0$ through a two-dimensional matrix of N randomly distributed circular obstacles with radius R . The obstacles are placed in a square with linear dimension L , assuming periodic boundary conditions both in x and y direction. We consider systems with obstacle densities $\rho = 0.0012, 0.012, 0.1963, 0.3927, 0.5890, \text{ and } 0.7853$ (for the definition of ρ , see Sec. II). The tracer particle is subjected to a uniform magnetic field B that acts perpendicular to the plane of motion. The absolute value of its velocity is fixed to $v_0 = 1.0$. In the absence of obstacles the tracer particle performs a circular motion with cyclotron frequency ω_{cy} (see above) and the cyclotron radius $R_{cy} = v_0/\omega_{cy}$. Below, we use a reduced magnetic field \tilde{B} , defined by $\tilde{B} = B/B_0$ with $B_0 = m^*v_0/(eR)$. In terms of this reduced magnetic field, the cyclotron radius can be written as $R_{cy} = R/\tilde{B}$.

In the simulation, one obtains the conductivity tensor via the calculation of the diffusion tensor \mathbf{D} . The elements of this tensor D_{ij} (with $i, j = x, y$) are given by the Green-Kubo relation [1]

$$D_{ij} = \int_0^\infty dt \langle v_i(0)v_j(t) \rangle, \quad (10)$$

where $\langle \dots \rangle$ denotes an ensemble average. Note that for the diffusion coefficients D_{ij} the relations $D_{xx} = D_{yy}$ and $D_{xy} = -D_{yx}$ hold. For a degenerate Fermi gas in two dimensions, the elements of the diffusion tensor can be related to the conductivity tensor via

$$\sigma_{ij} = \frac{2n_e e^2}{m^* v_0^2} D_{ij}, \quad (11)$$

with n_e the density of electrons. Interactions between the electrons are neglected throughout our study. The conductivities σ_{ij} can be directly extracted from the experimental data. Therefore, the diffusion coefficients D_{ij} from the simulation are converted to the σ_{ij} 's using Eq. (11).

Figure 1 displays typical trajectories for different densities, at each density for $\tilde{B} = 0.05$ (red lines) and $\tilde{B} = 0.15$ (blue lines). In the following, our focus is on the magnetotransport at low \tilde{B} fields where the cyclotron radius is large compared to the obstacle radius of the tracer particle. The considered obstacle densities are below the percolation threshold at $\rho_c \approx 1.128$. Above this threshold, i.e., for $\rho > \rho_c$, the tracer particle is localized and both σ_{xx} and σ_{xy} vanish. In the presence of a magnetic field, at a given density $\rho < \rho_c$, there is a second localization transition that occurs at a critical field $\tilde{B}_c = (\sqrt{\rho_c/\rho} - 1)^{-1}$. For $\tilde{B} > \tilde{B}_c$, the conductivity σ_{xx} vanishes. However, the magnetoconductivity σ_{xy} remains finite and, as shown by Kuzmany and Spohn [40], is inversely proportional to the magnetic field, $\sigma_{xy} \propto \tilde{B}^{-1} e^{\pi\rho}$. As a consequence, the ansatz (12) is expected to fail when one approaches \tilde{B}_c and is certainly incorrect for $\tilde{B} > \tilde{B}_c$. Indeed, this behavior is confirmed by our data (see below).

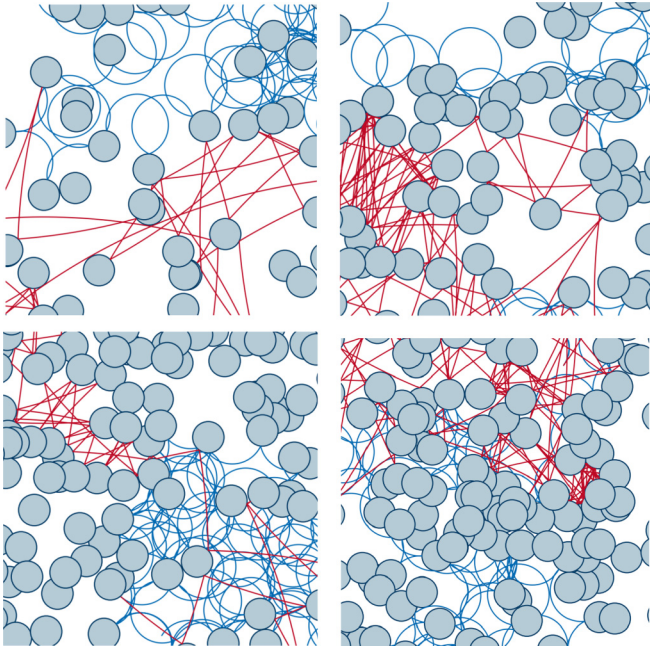


FIG. 1. Snapshots of trajectories from the simulation at $\tilde{B} = 0.05$ (red lines) and $\tilde{B} = 0.15$ (blue lines) for the densities $\rho = 0.1963$ (upper-left panel), $\rho = 0.3927$ (upper-right panel), $\rho = 0.5890$ (lower-left panel), and $\rho = 0.7853$ (lower-right panel).

IV. EXPERIMENTAL SETUP AND MEASUREMENT TECHNIQUES

A GaAs/Al_{0.3}Ga_{0.7}As heterostructure containing a two-dimensional electron gas (2DEG) 150 nm below the surface is used. At liquid helium temperatures, the pristine 2DEG has an electron density around $n_e = 2.42 \times 10^{15} \text{ m}^{-2}$ as determined from the Shubnikov-de Haas (SdH) oscillations (see below), and a typical electron mobility around $340 \text{ m}^2/\text{Vs}$, which depends somewhat on the position of the array on the wafer and on the cooldown. The corresponding Fermi velocity and mean-free path are $v_0 = 2.17 \times 10^5 \text{ m/s}$ and $\Lambda_e = 31 \text{ }\mu\text{m}$, respectively. The Lorentz arrays are patterned into sections of the Hall bar and have an area of $120 \text{ }\mu\text{m} \times 100 \text{ }\mu\text{m}$. The voltages are measured via probes of $10 \text{ }\mu\text{m}$ width and with a separation of $100 \text{ }\mu\text{m}$. The preparation of the Lorentz arrays has been described in detail elsewhere [41]. In brief, circular indentations of $\approx 150 \text{ nm}$ depth and at random positions have been patterned by electron beam lithography and subsequent reactive ion etching. Due to a lateral depletion length of approximately 75 nm , their actual relevant radius is accordingly larger than the lithographic one, amounting to 500 nm . The reduced obstacle densities of the arrays correspond to those also chosen in the simulation (see above). A scanning electron microscope picture of the sample at $\rho = 0.1963$ is shown in Fig. 2. It should be mentioned that the observation of memory effects is also possible on other types of random but static potential landscapes [42–44].

The transport measurements are carried out in the mixing chamber of a $^3\text{He}/^4\text{He}$ dilution refrigerator with a base temperature of 25 mK as well as in a ^4He gas flow cryostat for temperatures above 1.2 K . Both cryostats are equipped with superconducting solenoids with maximum magnetic fields

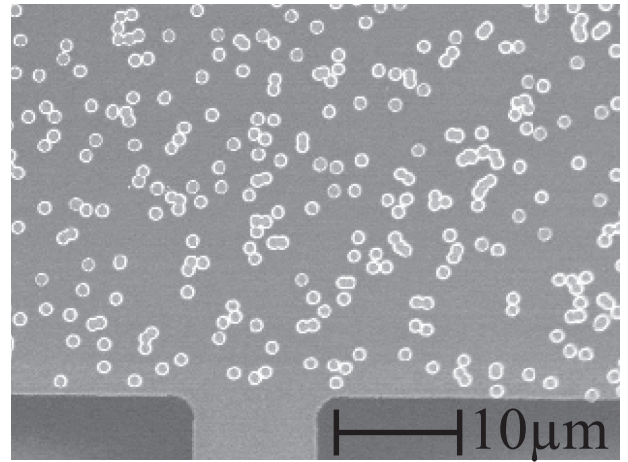


FIG. 2. Scanning electron microscope picture of a section of the sample with $\rho = 0.1963$. The bright area corresponds to the Hall bar and a voltage probe containing the two-dimensional electron gas, which is removed by an etch step in the dark regions.

above $B = 8 \text{ T}$. An AC current of amplitude 500 nA and a frequency of 17.7 Hz is applied, and the voltage drops across the arrays in longitudinal (x) and transverse (y) directions are recorded via the voltage probes using lock-in amplifiers (SR 830 from Stanford Instruments). All data shown are obtained by sweeping the magnetic field across its zero point and subsequent symmetrization for $\rho_{xx}(B)$ and antisymmetrization for $\rho_{xy}(B)$, respectively, in order to eliminate possible mutual admixtures. The data shown for $d\rho_{xy}/dB$ are numerical derivatives of the antisymmetrized measurements of $\rho_{xy}(B)$. The sharp peak of $\rho_{xx}(B)$ at $B = 0$ allows us an accurate determination of the magnetic field offset of about 0.2 mT in our system, most likely due to some magnetic flux trapping. Figure 3 shows the Hall resistance ρ_{xy} as a function of the magnetic field B at different temperatures T for the density $\rho = 0.589$. Here, we display on the upper axis of abscissae the reduced magnetic field $\tilde{B} = B/B_0$ with $B_0 = 165.2 \text{ mT}$ (to compute B_0 , we have assumed that the effective electron mass is $m^* = 6.097 \times 10^{-32} \text{ kg}$). For each temperature, one can identify an initial linear regime of the function $\rho_{xy}(B)$ at sufficiently low B field. The range of this linear regime increases with increasing temperature, accompanied by a decrease of the slope. This can be clearly inferred from the derivative $d\rho_{xy}(B)/dB(B)$ [Fig. 3(b)], using a logarithmic abscissa. Here, the constant that one can read off at small values of B corresponds to the Hall coefficient R_H . As is evident from the figure, with increasing temperature, R_H approaches the Drude-Hall coefficient $R_{DH} = 2.44 \times 10^3 \text{ }\Omega/\text{T}$ (marked by the horizontal bold black line). With increasing temperature, the scattering of the electrons by phonons becomes more and more important and thus our result indicates that phonons lead to a randomization of the electron motion, i.e., successive collisions of electrons with the obstacles tend to become uncorrelated. As a consequence, the Drude model seems to hold at sufficiently high temperature (at our highest temperature, $T = 32 \text{ K}$, we find the Hall coefficient $R_H \approx 2.63 \times 10^3 \text{ }\Omega/\text{T}$, which is already close to the Drude-Hall value $R_{DH} \approx 2.44 \times 10^3 \text{ }\Omega/\text{T}$). In the following, we only consider

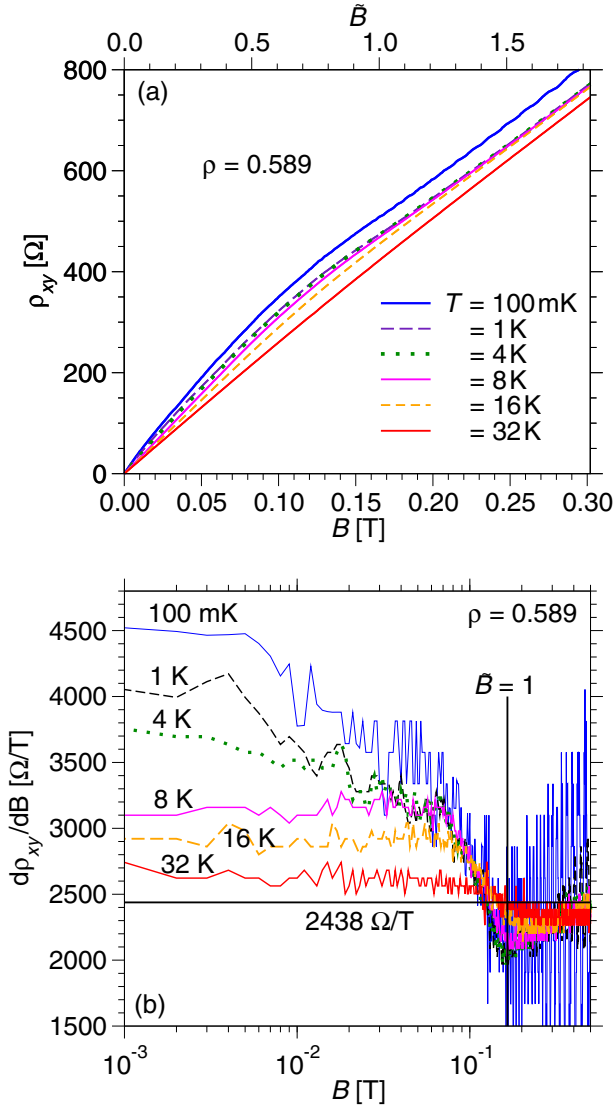


FIG. 3. (a) Hall resistance ρ_{xy} , as obtained from the experiment, as a function of the magnetic field B in unit of Tesla (lower axis of abscissae) and the reduced magnetic field \tilde{B} (upper axis of abscissae) at different temperatures T for the array with $\rho = 0.589$. (b) Derivative $d\rho_{xy}/dB$ in Fig. 3(b) corresponding to the data in (a). The horizontal black line at $2438 \Omega/T$ corresponds to the value of the Drude-Hall coefficient R_{DH} . The vertical black line marks $\tilde{B} = 1.0$. Adapted from Ref. [41].

the data measured at the lowest temperature, $T = 100$ mK. At this temperature, one may assume that any contributions from electron-phonon scattering processes can be neglected and thus in this case the experiment approximates best the model considered in the simulations. Figure 3 indicates that the slope of ρ_{xy} does not lead to reliable estimates of the electron density n_e . This issue will be discussed in more detail below. However, reliable estimates of n_e can be obtained from the SdH oscillations that are evident, e.g., in the derivative $d\rho_{xy}/dB$ in Fig. 3(b) at $T = 100$ mK. These oscillations reflect the quantization of the electron gas in Landau levels with energies $E_j = (k - \frac{1}{2})\hbar\omega_{cy}$, $k = 0, 1, 2, 3, \dots$. To obtain n_e , we have analyzed the SdH oscillations in the magnetore-

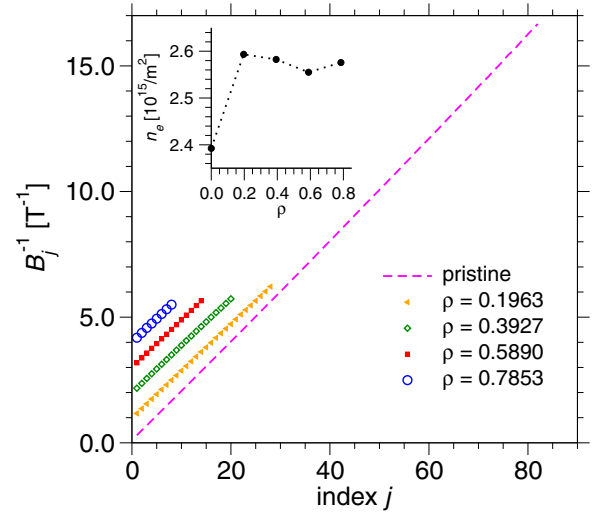


FIG. 4. Location of the SdH minima, B_j^{-1} , as a function of the index j for the pristine sample and the samples at the different obstacle densities (here, $j = 1$ just corresponds to the first minimum that can be identified). Note that the data are shifted on the ordinate with increasing value of ρ in steps of $1 T^{-1}$. The inset shows the electron density n_e as function of ρ , resulting from the slope of B_j^{-1} .

sistance ρ_{xx} (see below). One expects [45,46] that ρ_{xx} has a SdH minimum whenever a multiple j of $\hbar\omega_{cy}$ is equal to the Fermi energy $E_F = \pi\hbar^2 n_e/m^*$. Hence, the equation $B_j^{-1} = j e / (\pi\hbar n_e)$ holds. The derivative of this equation with respect to j gives $s \equiv dB_j^{-1}/dj = e / (\pi\hbar n_e)$ and thus $n_e = e / \pi\hbar s$. Figure 4 shows B_j^{-1} as a function of j for a pristine sample and the samples for the different densities. The pristine sample is an unpatterned Hall bar of identical geometry, integrated in the chip that hosts the four Lorentz arrays. From the slopes of $B_j^{-1}(j)$, we have determined the electron density n_e as function of density ρ (inset of Fig. 4). While we obtain an electron density around $n_e = 2.58 \times 10^{15} m^{-2}$ for the samples with finite obstacle density ρ , a significant lower value of $n_e \approx 2.39 \times 10^{15} m^{-2}$ is found for the pristine samples. This indicates that the etching step reduces the number of doping electrons captured in the surface states, which therefore contribute to the electron density in the 2DEG.

V. RESULTS ON THE MAGNETOTRANSPORT

In this section, we present the results on the magnetotransport, as obtained from experiment and simulation. As a reference, we first analyze the simulation results at very low obstacle densities as well as those from the experiment for the pristine sample. Here, we check to what extent the low density data can be described in the framework of the DB model. Then, we investigate the behavior at intermediate and high density to see how memory effects affect the transport properties, in particular with respect to the behavior of the Hall resistance at low magnetic field.

A. Low obstacle densities

For the analysis of the transport at intermediate and high density, it is useful to first get an idea about the density range

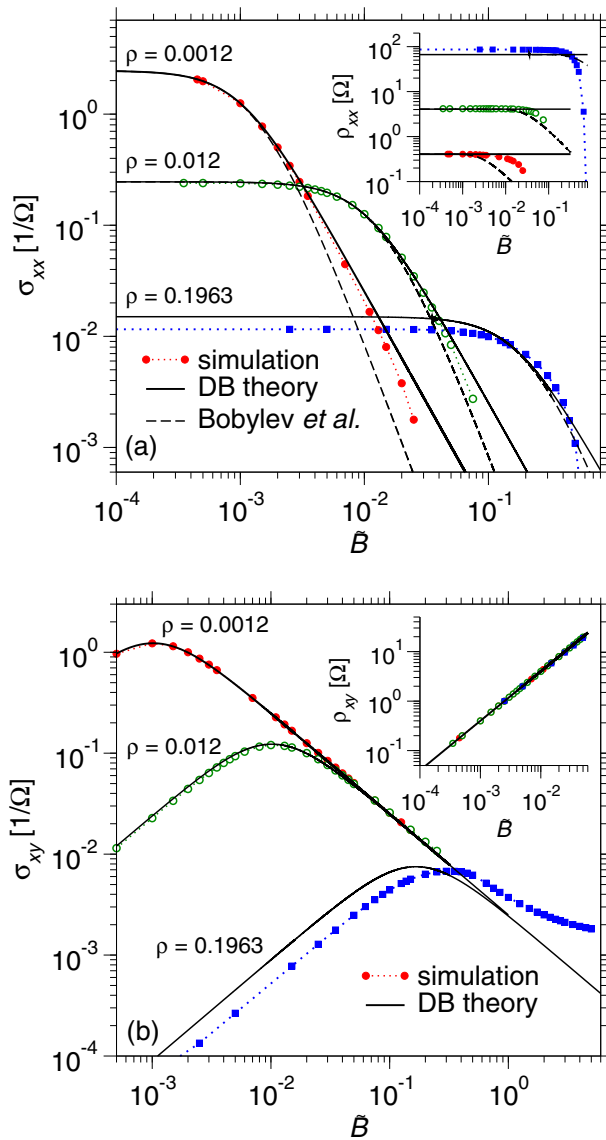


FIG. 5. (a) Conductivity σ_{xx} as a function of \tilde{B} for the densities $\rho = 0.0012, 0.012,$ and 0.1963 . The results of the simulation are compared to the predictions of the DB theory, Eq. (2), and the theory of Bobylev *et al.* [2], Eq. (7). The inset shows the corresponding data for the magnetoresistance ρ_{xx} . (b) Same as in (a), but now for the magnetoconductivity σ_{xy} and the Hall resistance ρ_{xy} in the inset.

where the low-density theories are applicable. For $B = 0$, the DB theory (based on the LBE) provides an exact analytical formula for the conductivity in the Grad limit, see Eq. (4). Also in the presence of a magnetic field, both the LBE as well as the generalized Boltzmann equation [2] give analytical predictions for σ_{xx} , σ_{xy} , ρ_{xx} , and ρ_{xy} [cf. Eqs. (2)–(9)] that can be checked by the simulation without using any fit parameter. Below we refer to the results based on the generalized Boltzmann equation as Bobylev theory or Bobylev approach.

Figure 5 displays the comparison of simulation and theory for the obstacle densities $\rho = 0.0012, 0.012,$ and 0.1963 . Note that we do not show the results of the Bobylev theory for σ_{xy} and ρ_{xy} in Fig. 5(b) since they are very similar to the corresponding ones obtained from the DB theory. The different

quantities are plotted double-logarithmically as a function of the reduced magnetic field \tilde{B} . At the two lowest densities, the DB result is in quantitative agreement with the simulation if the value of \tilde{B} is significantly below the critical field \tilde{B}_c , which is at $\tilde{B}_c \approx 0.034$ for $\rho = 0.0012$ and at $\tilde{B}_c \approx 0.115$ for $\rho = 0.012$. This is remarkable since the DB theory outperforms the Bobylev approach, which, according to Refs. [2,32,37], is supposed to be exact in the Grad limit. For $\rho = 0.1963$, the conductivity σ_{xx} from the simulation exhibits a similar monotonic decay, as predicted by the DB theory, but there are significant quantitative differences between simulation and theory already at small magnetic fields. Thus, the density $\rho = 0.1963$ is beyond the low-density regime where the DB theory applies. However, the Hall resistance ρ_{xy} (inset of Fig. 5) seems to follow the same linear behavior on \tilde{B} for the three densities. Below we will see that this is different when approaching the regime of high densities. As we shall see now, the experimental pristine sample can be seen as a two-dimensional Lorentz gas at low density that can be well described by the DB theory. Here, the obstacles are impurities by which the electrons are scattered. Since we neither know the density of these impurities nor their effective size, we have to use the ratio R/ρ in Eqs. (2) and (3) for the DB theory and Eqs. (7) and (8) for the Bobylev theory as a fit parameter. Assuming $R/\rho = 55.5 \mu\text{m}$, we find excellent quantitative agreement of the DB results with the experimental data both for σ_{xx} and σ_{xy} as well as ρ_{xx} and ρ_{xy} (Fig. 6). The differences between experiment and theory of σ_{xy} as well as ρ_{xy} at low B fields are probably due to inaccuracies of the measurement around $B = 0$. For σ_{xx} as well as for ρ_{xx} , at $B \approx 0.1$ T the SdH oscillations set in. Of course, these oscillations cannot be described in the framework of the DB theory. However, the DB result seems to provide an “average curve” around which the SdH oscillations take place. Again we find that the Bobylev theory is worse than the DB theory in that it starts to strongly deviate from the experimental data of σ_{xx} and ρ_{xx} for $B \gtrsim 0.002$ T. For σ_{xy} and ρ_{xy} , DB and Bobylev theory are very similar and therefore we do not show the results of the Bobylev theory in Fig. 6(b).

B. Intermediate and high obstacle densities

The density range at which memory effects become important and at which the DB theory starts to fail on a qualitative level can be identified from the behavior of the conductivity σ_{xx} . Figure 7 shows $\sigma_{xx}(B)/\sigma_{xx}(B=0)$, as obtained from experiment (solid lines) and simulation (circles), as a function of \tilde{B} for different densities ρ in a double-logarithmic plot. For the low densities ($\rho = 0.012$ for the simulation and experimental pristine sample), we observe a quick decay that is well described by the DB theory. For $\rho \geq 0.1963$ and at small magnetic fields, $\tilde{B} \lesssim 0.1$, there is a very weak dependence of $\sigma_{xx}/\sigma_{xx}(B=0)$ on \tilde{B} , i.e., the value of σ_{xx} is very close to that at $\tilde{B} = 0$ for each of the considered densities. At $\rho = 0.1963$ and $\rho = 0.3927$, the weak dependence on \tilde{B} is followed by a monotonous decrease of σ_{xx} with increasing \tilde{B} while at larger densities (here, $\rho \geq 0.589$), the diffusion coefficient increases up to a maximum before it decreases monotonically at larger magnetic fields (for an explanation of this feature see Ref. [41]). Simulation and experiment are in good agreement for

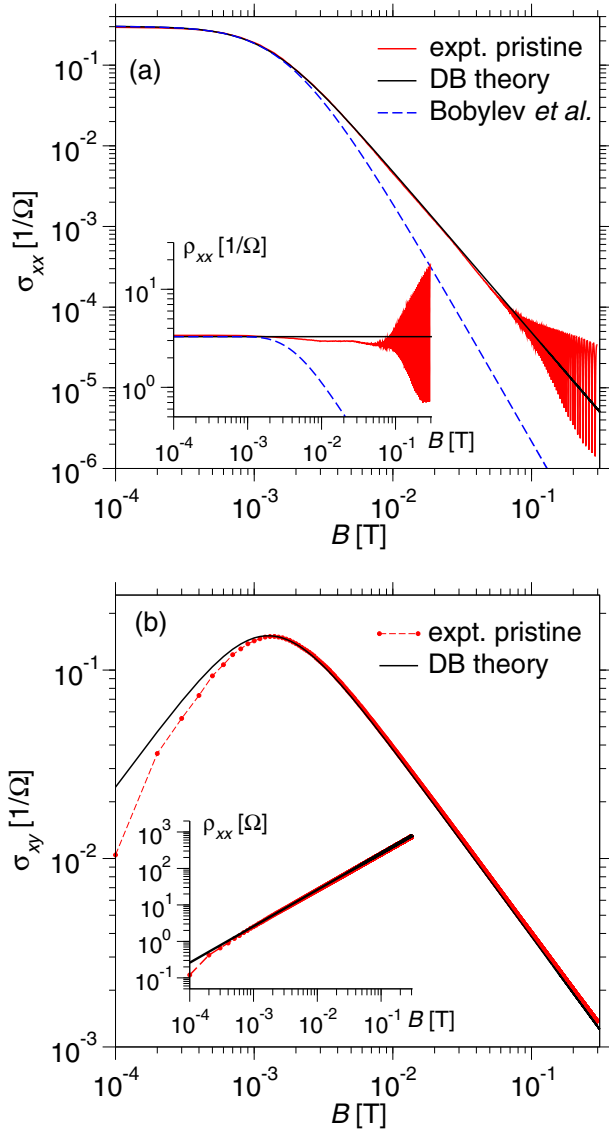


FIG. 6. (a) Conductivity σ_{xx} as a function of B for the experimental pristine sample in comparison to the DB theory, Eq. (2), and the theory of Bobylev *et al.* [2], Eq. (7). In the latter theoretical expressions, the ratio $R/\rho = 55.5 \mu\text{m}$ is used to obtain the best match with the experimental data (see text). The inset shows the corresponding data for the magnetoresistance ρ_{xx} . (b) Same as in (a), but now for the magnetoconductivity σ_{xy} and the Hall resistance ρ_{xy} in the inset.

$\tilde{B} \lesssim 1.0$. For larger values of \tilde{B} , the experimental data display a slower decay and quantum effects become important, as indicated by pronounced SdH oscillations. This quantum effect tends to enhance σ_{xx} when approaching the critical magnetic field \tilde{B}_c . In contrast to that, the simulation is purely classical and one observes a rapid decrease of σ_{xx} towards \tilde{B}_c . However, in the following, we are mainly interested in features at small magnetic fields, $\tilde{B} < 1.0$, i.e., the region of good agreement between simulation and experiment with respect to the quantity $\sigma_{xx}(B)/\sigma_{xx}(B=0)$. In the framework of the DB model, there is a simple relationship between σ_{xx} and the Hall conductivity σ_{xy} . As can be inferred from Eqs. (2) and (3), in

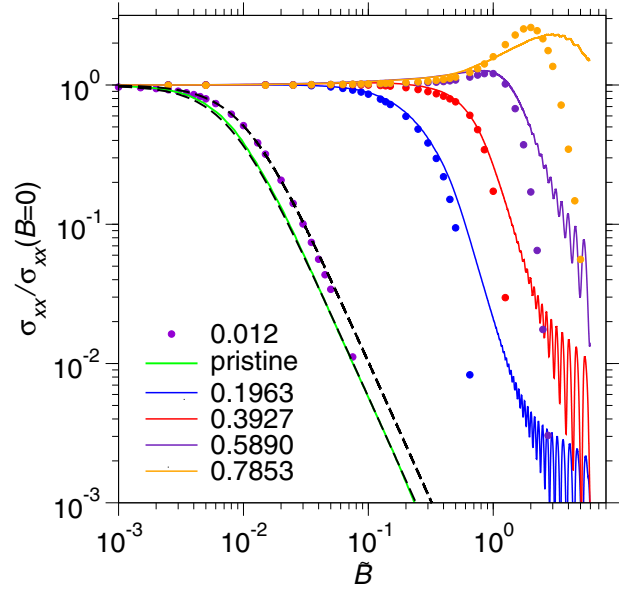


FIG. 7. Comparison between experiment (solid lines) and simulation (circles) for the reduced conductivity $\sigma_{xx}/\sigma_{xx}(B=0)$ as a function of \tilde{B} for $\rho = 0.1963, 0.3927, 0.5890$, and 0.7853 . Also included are the data of the pristine sample and the simulation at $\rho = 0.012$, both in comparison to DB theory (dashed black lines).

this case the relation

$$\sigma_{xy} = \omega_{cy} \tau \sigma_{xx} \quad (12)$$

holds for arbitrary values of B . Note that we have replaced τ_{Dr} by τ in Eq. (12), because in the following we use this equation to analyze simulation and experiment at obstacle densities far beyond the low-density limit. Then, Eq. (12) still holds for sufficiently low magnetic fields and allows to extract the diffusive time scale τ .

As for low densities, the Hall conductivity σ_{xy} is of course zero at $\tilde{B} = 0$ and it increases with increasing \tilde{B} up to a maximum, the location of which moves to larger values of \tilde{B} with increasing density ρ [see Fig. 8(a) for the experiment and Fig. 8(b) for the simulation]. The validity of Eq. (12) for low values of \tilde{B} is demonstrated in Fig. 8 for $\rho \geq 0.1963$. Here, the solid lines correspond to the quantity $\omega_{cy} \tau \sigma_{xx}$ where the parameter τ is a “fit parameter”, used to obtain the best agreement between σ_{xy} and $\omega_{cy} \tau \sigma_{xx}$ at low values of \tilde{B} . Note that the values of τ are indicated in Fig. 8 for the different densities. In order to obtain τ from the experimental as well as the simulation data, we have used the equation

$$\tau = \lim_{\tilde{B} \rightarrow 0} \frac{1}{\omega_{cy}} \frac{\sigma_{xy}}{\sigma_{xx}} = \lim_{\tilde{B} \rightarrow 0} \frac{R}{\tilde{B} v_0} \frac{\sigma_{xy}}{\sigma_{xx}}. \quad (13)$$

Then, the idea is to read off τ from plots of the right-hand side of this equation as a function of \tilde{B} for $\tilde{B} \rightarrow 0$. As Fig. 8 shows, for the experiment as well as for the simulation, Eq. (12) holds up to values of \tilde{B} with $\omega_{cy} \tau \approx 0.5$.

The failure of Eq. (12) can be interpreted—at least for intermediate magnetic field strengths \tilde{B} —in terms of a \tilde{B} -dependent effective time scale τ_{eff} . At low values of \tilde{B} , both in experiment and simulation this time scale decreases with increasing \tilde{B} . At higher values of \tilde{B} , the behavior of τ_{eff} is

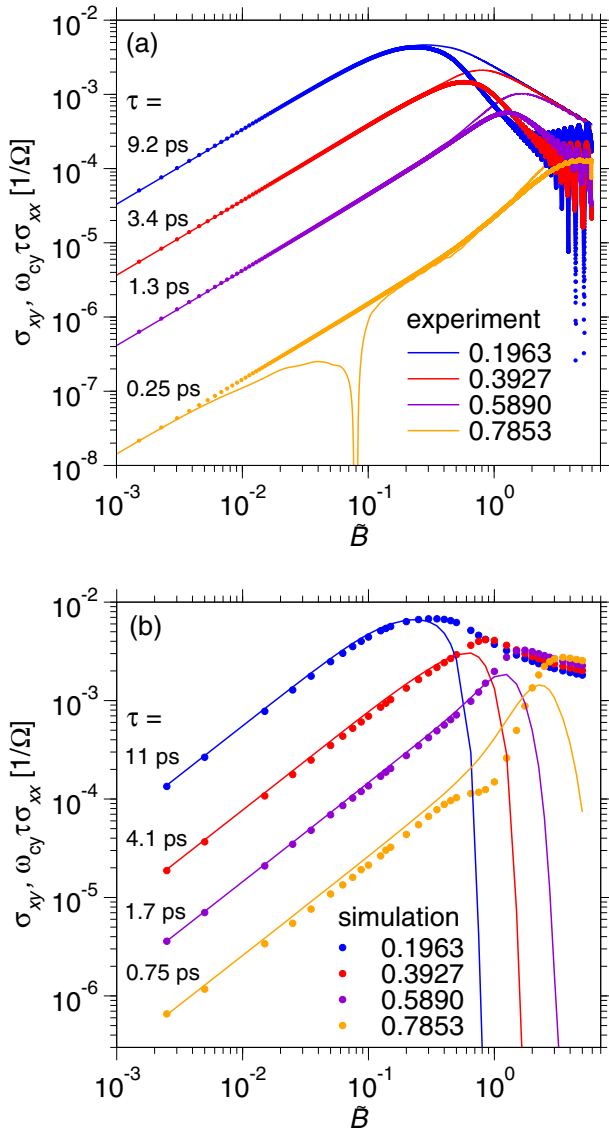


FIG. 8. Hall conductivity σ_{xy} (circles) and $\omega_{cy}\tau\sigma_{xx}$ (solid lines) as a function of \tilde{B} for different densities for (a) the experiment and (b) the simulation. The values of τ are indicated in both panels.

different in experiment and simulation. In the simulation, σ_{xx} vanishes in the limit $\tilde{B} \rightarrow \tilde{B}_c$ while $\sigma_{xy} \propto \tilde{B}^{-1}$ for $\tilde{B} > \tilde{B}_c$ (see Ref. [40]). This is reflected in the behavior of the simulation data at large values of \tilde{B} . Here, the quantity $\omega_{cy}\tau\sigma_{xx}$ exhibits a rapid decrease at large magnetic fields while, for all the densities, σ_{xy} displays only a mild decrease with increasing magnetic field. In the experiment, $\omega_{cy}\tau\sigma_{xx}$ is slightly larger than σ_{xy} at high value of \tilde{B} , with σ_{xy} showing pronounced SdH oscillations. Note that the singular behavior around $\tilde{B} \approx 0.08$, that is seen in the experimental data for the highest density, $\rho = 0.7853$, is an artifact. We attribute this to an obstacle configuration close to one voltage probe that may cause imperfect coupling of the probe to the Hall bar in this magnetic field range. The time τ , scaled with the Drude time τ_{Dr} , and the reduced conductivity $\sigma_{xx}(\tilde{B} = 0)/\sigma_0$ at zero magnetic field as a function of density are shown in Fig. 9 for the experiment and the simulation (see Sec. II for the definition of τ_{Dr}

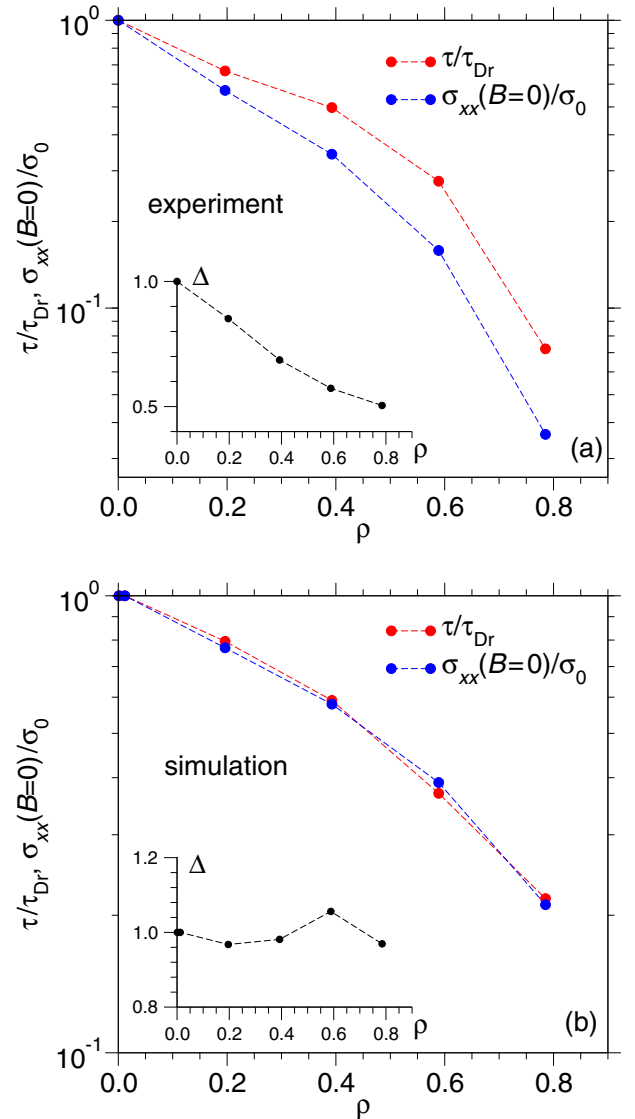


FIG. 9. Reduced diffusive time τ/τ_{Dr} and reduced conductivity $\sigma_{xx}(\tilde{B} = 0)/\sigma_0$ as a function of ρ for (a) the experiment and (b) the simulation. The insets show $\Delta = \sigma_{xx}(\tilde{B} = 0)\tau_{Dr}/(\tau\sigma_0)$ as a function of ρ .

and σ_0). The figures indicate that τ/τ_{Dr} and $\sigma_{xx}(\tilde{B} = 0)/\sigma_0$ have a similar functional behavior on ρ , which is consistent with the interpretation that τ describes a diffusive time scale. For the simulation [Fig. 9(b)], both τ/τ_{Dr} and $\sigma_{xx}(\tilde{B} = 0)/\sigma_0$ essentially fall onto one curve, as expected. This is also indicated in the inset of Fig. 9(b), showing the ratio $\Delta = \sigma_{xx}(\tilde{B} = 0)\tau_{Dr}/(\tau\sigma_0)$, which is roughly equal to one in the considered range of densities. For the experiment [Fig. 9(a)], the values that we find for τ/τ_{Dr} and $\sigma_{xx}(\tilde{B} = 0)/\sigma_0$ are of the same order of magnitude as those in the simulation. However, the ratio $\sigma_{xx}(\tilde{B} = 0)/\sigma_0$ lies significantly below τ/τ_{Dr} over the whole density range. We will get back to this deviation in the discussion of Fig. 13. The ratio Δ , as extracted from the experiment, is equal to one in the limit $\rho \rightarrow 0$ and it monotonically decreases to about 0.5 at large density. The observed relationship between σ_{xx} and σ_{xy} can be used to

reveal the \tilde{B} dependence of the magnetoresistance ϱ_{xx} and the Hall resistance ϱ_{xy} in the range of small magnetic fields \tilde{B} . These quantities can be obtained from a matrix inversion of the conductivity tensor and are given by

$$\varrho_{xx} = \frac{\sigma_{xx}}{\sigma_{xx}^2 + \sigma_{xy}^2}, \quad (14)$$

$$\varrho_{xy} = \frac{\sigma_{xy}}{\sigma_{xx}^2 + \sigma_{xy}^2}. \quad (15)$$

Using Eq. (12), which, according to our results shown in Fig. 8, is a good approximation for $\omega_{cy}\tau \leq 0.5$, we can eliminate σ_{xy} from Eqs. (14) and (15) and express ϱ_{xx} and ϱ_{xy} in terms of σ_{xx} ,

$$\varrho_{xx} = \frac{1}{1 + \omega_{cy}^2 \tau^2} \frac{1}{\sigma_{xx}}, \quad (16)$$

$$\varrho_{xy} = \frac{\omega_{cy}\tau}{1 + \omega_{cy}^2 \tau^2} \frac{1}{\sigma_{xx}}. \quad (17)$$

According to Eq. (17), the leading-order term of ϱ_{xy} in the limit of small B is given by

$$\varrho_{xy} \approx \frac{\omega_{cy}\tau}{\sigma_{xx}(B=0)} = \frac{e\tau B}{m^* \sigma_{xx}(B=0)} = R_H B \quad (18)$$

$$= \tilde{R}_H \tilde{B} \quad (19)$$

where we have introduced the Hall coefficients with respect to the proportionality to B ,

$$R_H = \frac{e\tau}{m^* \sigma_{xx}(B=0)}, \quad (20)$$

and to \tilde{B} ,

$$\tilde{R}_H = R_H B_0. \quad (21)$$

If one inserts the result from Drude theory for the conductivity $\sigma_{xx}(B=0)$ in Eqs. (20) and (21), one obtains $R_{DH} = 1/(n_e e)$ and $\tilde{R}_{DH} = B_0/(n_e e)$. Figures 10(a) and 10(b) show ϱ_{xx} at the different densities, as obtained from the experiment and simulation, respectively. Also included in these plots is the approximation (16). Its range of validity obviously depends on density. While for $\rho = 0.1963$ it holds for $\tilde{B} \lesssim 0.2$, for the largest density, $\rho = 0.7853$, it seems to be a good approximation up to values above $\tilde{B} = 1.0$. A fair agreement between experiment and simulation is found. For small \tilde{B} , quite similar values for ϱ_{xx} are obtained while significant deviations between simulation and experiment occur for large \tilde{B} fields, which are due to the approach of the localization transition in the simulation, which is strongly rounded in the experiment, in part due to the presence of quantum effects such as SdH oscillations (cf. the discussion in Refs. [41,47]). In Figs. 11 and 12, we show the dependence of the Hall resistance ϱ_{xy} on the magnetic field \tilde{B} at the different obstacle densities for the experiment and the simulation, respectively. In these plots, we have also included the Hall resistance, as obtained from Eq. (17), and the linear approximation, Eq. (21), that is expected to hold at very low magnetic fields. In all cases, the approximation (17) works well at least up to magnetic fields of the order of $\tilde{B} \approx 0.2$, while the linear behavior (21) is asymptotically reached for very small values of \tilde{B} (cf. the insets in Figs. 11 and 12). Again, the experimental data for the

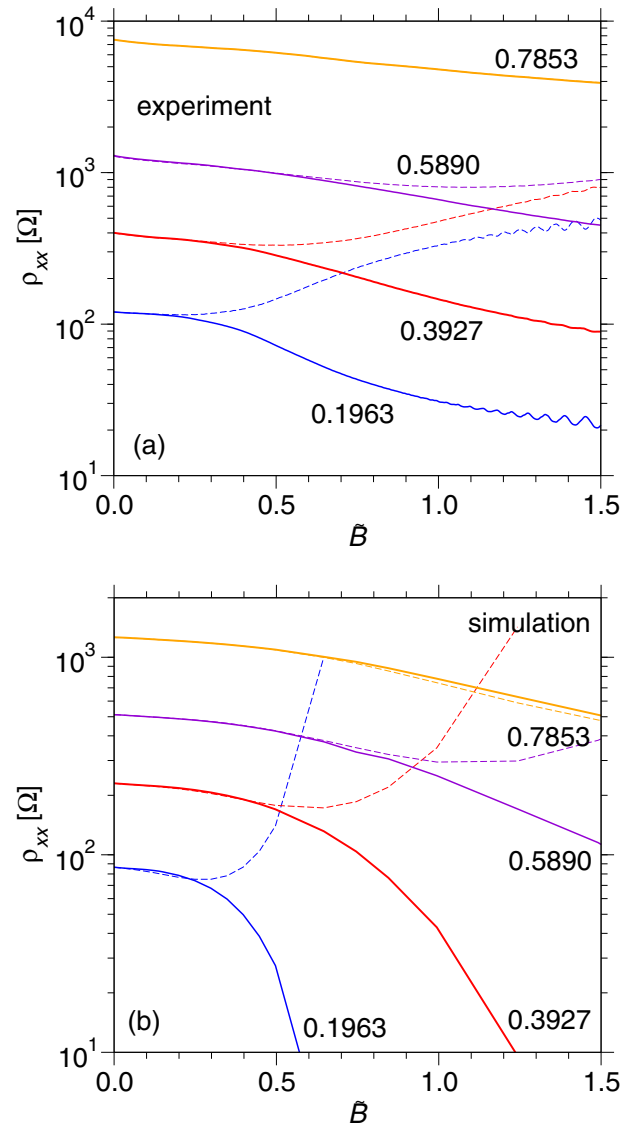


FIG. 10. Magnetoresistance $\varrho_{xx}(\tilde{B})$ at different densities, as obtained from (a) the experiment and (b) the simulation. Solid lines correspond to the data while the dashed lines are calculated via Eq. (16).

highest density, $\rho = 0.7853$ [see Fig. 11(d)] are not reliable over the full parameter range.

In Fig. 13, the Hall coefficient \tilde{R}_H , as obtained from the Hall resistance data in Figs. 11 and 12 in the limit $B \rightarrow 0$, is plotted as a function of obstacle density ρ . In the simulation, \tilde{R}_H decreases by about 15% in the considered range of densities. Towards $\rho \rightarrow 0$, the simulation data are consistent with the result from Drude theory $\tilde{R}_{DH} \approx 427.0 \Omega$, assuming an electron density $n_e = 2.42 \times 10^{15} \text{ m}^{-2}$, as used above for the conversion from D_{ij} to σ_{ij} . For $\rho \geq 0.1963$, the value $n_e = 2.58 \times 10^{15} \text{ m}^{-2}$ was used, according to the estimate from the SdH oscillations in Fig. 4 and the corresponding evolution of the Drude-Hall coefficient \tilde{R}_{DH} with density (blue curve in Fig. 13). Note that even on a qualitative level the findings in Figs. 12 and 13 are not in agreement with the theory of Dmitriev *et al.* [33,34]. The experimental data also

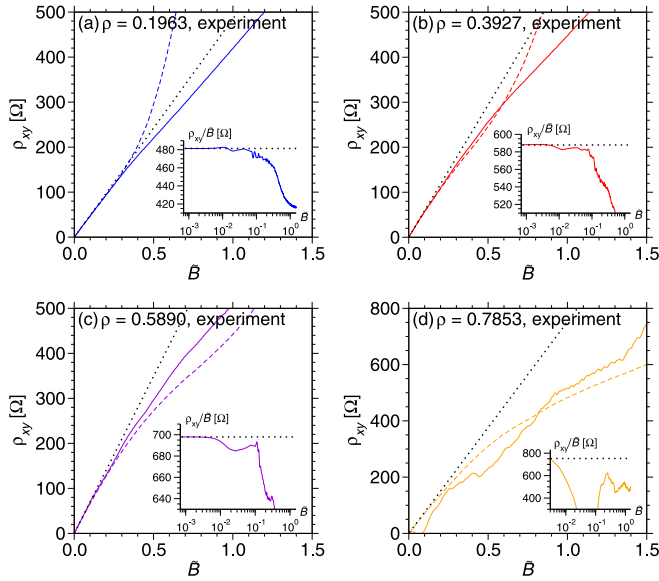


FIG. 11. Hall resistance $\rho_{xy}(\tilde{B})$, as obtained from the experiment, at the densities (a) $\rho = 0.1963$, (b) $\rho = 0.3927$, (c) $\rho = 0.5890$, and (d) $\rho = 0.7853$. The solid lines represent the data, while the blue dashed lines are calculated via Eq. (17). The black dotted lines represent the expected behavior at low magnetic fields, $\rho_{xy} = \tilde{R}_H \tilde{B}$ with the Hall coefficient \tilde{R}_H given by Eq. (21). The insets display ρ_{xy}/\tilde{B} . At sufficiently low magnetic field, this quantity is supposed to approach Hall coefficient \tilde{R}_H (the corresponding constant is shown as a dotted horizontal line in these plots).

approaches the value of the Drude theory in the limit $\rho \rightarrow 0$. However, unlike \tilde{R}_H from the simulation, the experimentally determined Hall coefficient increases with increasing density. The reasons for this deviation are presently not well understood. We note, however, that several well-established effects, that contribute to the magnetoconductivity close to $B = 0$, may remain visible in ρ_{xy} as well, for example interaction

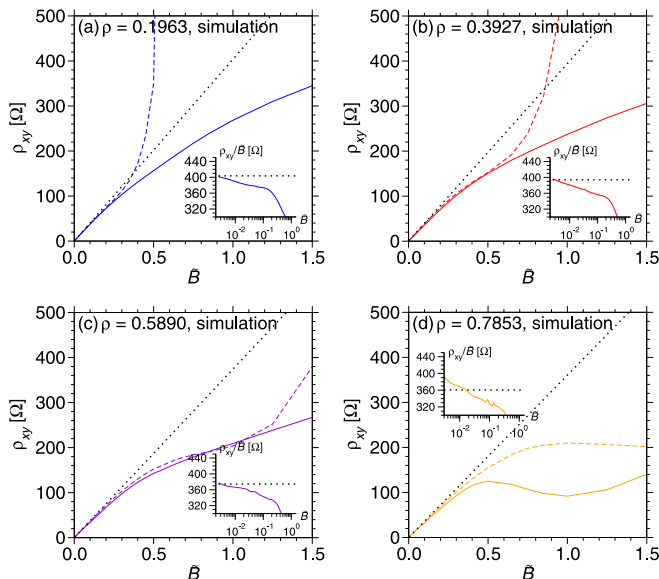


FIG. 12. Same as Fig. 11 but now for the simulation.

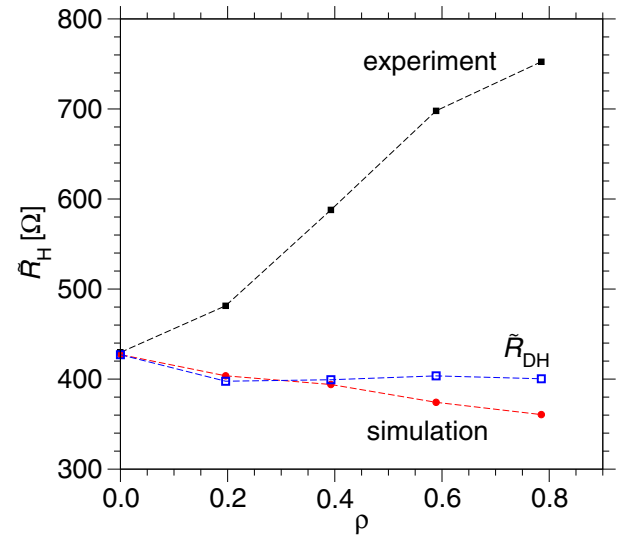


FIG. 13. Reduced Hall coefficient \tilde{R}_H as a function of density for experiment and simulation. Also displayed is the coefficient $\tilde{R}_{DH} = B_0/(n_e e)$, as expected from Drude theory, taking the estimates of n_e , as obtained from the analysis of the SdH oscillations (see inset of Fig. 4).

corrections [48], nonspecular scattering at the edges of the Hall bar [49], or smooth background disorder [50].

VI. SUMMARY AND CONCLUSIONS

We have studied the magnetotransport in a two-dimensional disordered Lorentz gas with circular obstacles, using a combination of experiment and simulation. The aim of our study is to elucidate the Hall resistance ρ_{xy} at obstacle densities ρ that go beyond the low-density limit where in the classical limit the DB theory is expected to hold. The central ansatz, used in our paper, is the relationship $\sigma_{xy} = \omega_{cy} \tau \sigma_{xx}$, which is inspired by the Drude model, cf. Eq. (12). For $\tilde{B} > \tilde{B}_c$ (with \tilde{B}_c the critical magnetic field), the Hall conductivity σ_{xy} is expected to be finite [40] with a relatively weak dependence on the magnetic field $\propto 1/\tilde{B}$, while the conductivity σ_{xx} vanishes for $\tilde{B} > \tilde{B}_c$. Therefore, Eq. (12) cannot be correct around and above \tilde{B}_c . In the experiment, the localization transition at \tilde{B}_c is rounded and “masked” by quantum effects, i.e., the onset of Landau quantization, as well as by residual scattering.

Despite the limitation of the ansatz (12), we have found a significant range of \tilde{B} values where it holds. Here, the deviations to the DB theory, in our case associated with classical memory effects, can be understood in terms of the diffusive time scale τ . As expected, at $\tilde{B} = 0$, this time scale has a similar dependence on density ρ as the conductivity $\sigma_{xx}(\tilde{B} = 0)$ (see Fig. 9). With increasing \tilde{B} , both in simulation and experiment, the time τ tends to decrease. This is reflected, e.g., in our finding that the approximation (17) overestimates the “exact” data for ρ_{xy} (Figs. 11 and 12). In the simulation, the Hall coefficient \tilde{R}_H has a relatively weak dependence on ρ . This can be explained by the fact that within our framework, \tilde{R}_H is proportional to $\tau/\sigma_{xx}(\tilde{B} = 0)$ and this ratio is only weakly dependent on density (see Fig. 9).

In the experiment, unlike the simulation, \tilde{R}_H increases with increasing density ρ . This is attributed to additional experimental influences like the finite magnetic field resolution, residual scattering as well as quantum effects. Nevertheless, the strong suppression of the Hall slope close to $B = 0$ is clearly visible in the experiment as well, indicating that in the presence of memory effects, the Hall slope is no longer suited to extract the carrier density. Moreover, our experiments indicate that $R_H \neq (en_e)^{-1}$ over the full classical magnetic field range and approaches this value only as the temperature or the magnetic field is strongly increased. Furthermore, the results reported here are related to studies of the giant negative magnetoresistance (GNMR), where a negative longitudinal

magnetoresistivity is observed, the temperature-independent part of which is usually attributed to scattering on sparse but strong obstacles, which thus form a Lorentz gas with inhomogeneous obstacle shapes and sizes [51–55], originating, for example, from oval defects [44]. It may be worth studying whether the type of nonlinearities in $\varrho_{xy}(B)$ can be observed in such systems. An interesting issue is the Hall effect in Ehrenfests' windtree model where the obstacles are equally oriented squares instead of circles. Here, in the absence of a magnetic field, the conductivity σ_{xx} vanishes at any finite density [56]. This leads to an anomalous nonlinear behavior of the Hall resistance at small magnetic field, as shown in a forthcoming study.

-
- [1] J. R. Dorfman, H. van Beijeren, and T. R. Kirkpatrick, *Contemporary Kinetic Theory of Matter* (Cambridge University Press, Cambridge, 2021).
- [2] A. Bobylev, F. A. Maaø, A. Hansen, and E. Hauge, *J. Stat. Phys.* **87**, 1205 (1997).
- [3] E. H. Hall, *London, Edinburgh Dublin Philos. Mag. J. Sci.* **12**, 157 (1881).
- [4] K. v. Klitzing, G. Dorda, and M. Pepper, *Phys. Rev. Lett.* **45**, 494 (1980).
- [5] D. C. Tsui, H. L. Stormer, and A. C. Gossard, *Phys. Rev. Lett.* **48**, 1559 (1982).
- [6] R. B. Laughlin, *Phys. Rev. Lett.* **50**, 1395 (1983).
- [7] B. L. Altshuler, D. Khmel'nitzkii, A. I. Larkin, and P. A. Lee, *Phys. Rev. B* **22**, 5142 (1980).
- [8] M. A. Khodas and A. M. Finkel'stein, *Phys. Rev. B* **68**, 155114 (2003).
- [9] G. M. Minkov, O. E. Rut, A. V. Germanenko, A. A. Sherstobitov, V. I. Shashkin, O. I. Khrykin, and B. N. Zvonkov, *Phys. Rev. B* **67**, 205306 (2003).
- [10] E. Galaktionov, A. Savchenko, and D. Ritchie, *Phys. Status Solidi C* **3**, 304 (2006).
- [11] K. E. J. Goh, M. Y. Simmons, and A. R. Hamilton, *Phys. Rev. B* **77**, 235410 (2008).
- [12] G. M. Minkov, A. V. Germanenko, O. E. Rut, A. A. Sherstobitov, and B. N. Zvonkov, *Phys. Rev. B* **82**, 035306 (2010).
- [13] H. Fukuyama, *J. Phys. Soc. Jpn.* **49**, 644 (1980).
- [14] A. M. Ortiz de Zavallos, N. C. Mamani, G. M. Gusev, A. A. Quivy, T. E. Lamas, and J. C. Portal, *Int. J. Mod. Phys. B* **21**, 1502 (2007).
- [15] V. J. Goldman, M. Shayegan, and H. D. Drew, *Phys. Rev. Lett.* **57**, 1056 (1986).
- [16] X. P. A. Gao, G. S. Boebinger, A. P. Mills, A. P. Ramirez, L. N. Pfeiffer, and K. W. West, *Phys. Rev. Lett.* **93**, 256402 (2004).
- [17] M. L. Roukes, A. Scherer, S. J. Allen, H. G. Craighead, R. M. Ruthen, E. D. Beebe, and J. P. Harbison, *Phys. Rev. Lett.* **59**, 3011 (1987).
- [18] A. K. Geim, I. V. Grigorieva, S. V. Dubonos, J. G. S. Lok, J. C. Maan, A. E. Filippov, and F. M. Peeters, *Nature (London)* **390**, 259 (1997).
- [19] S. Fasbender, J. Schluck, M. Cerchez, T. Heinzl, S. Sievers, K. Pierz, and H. W. Schumacher, *J. Appl. Phys.* **119**, 094302 (2016).
- [20] J. Jung, F. Zhang, and A. H. MacDonald, *Phys. Rev. B* **83**, 115408 (2011).
- [21] Z. Z. Du, H.-Z. Lu, and X. C. Xie, *Nat. Rev. Phys.* **3**, 744 (2021).
- [22] R. Fleischmann, T. Geisel, and R. Ketzmerick, *Europhys. Lett.* **25**, 219 (1994).
- [23] A. Y. Kuntsevich, A. V. Shupletsov, and M. S. Nunuparov, *Phys. Rev. B* **93**, 205407 (2016).
- [24] D. Weiss, M. L. Roukes, A. Menschig, P. Grambow, K. von Klitzing, and G. Weimann, *Phys. Rev. Lett.* **66**, 2790 (1991).
- [25] K. Ensslin and P. M. Petroff, *Phys. Rev. B* **41**, 12307 (1990).
- [26] A. Lorke, J. P. Kotthaus, and K. Ploog, *Phys. Rev. B* **44**, 3447 (1991).
- [27] K. Tsukagoshi, S. Wakayama, K. Oto, S. Takaoka, K. Murase, and K. Gamo, *Phys. Rev. B* **52**, 8344 (1995).
- [28] V. A. Tkachenko, O. A. Tkachenko, G. Minkov, and A. A. Sherstobitov, *JETP Lett.* **104**, 473 (2016).
- [29] A. Y. Kuntsevich, A. V. Shupletsov, and A. L. Rakhmanov, *Phys. Rev. B* **102**, 155426 (2020).
- [30] O. Yevtushenko, G. Lütjering, D. Weiss, and K. Richter, *Phys. Rev. Lett.* **84**, 542 (2000).
- [31] A. V. Bobylev, F. A. Maaø, A. Hansen, and E. H. Hauge, *Phys. Rev. Lett.* **75**, 197 (1995).
- [32] A. Bobylev, A. Hansen, J. Piasecki, and E. Hauge, *J. Stat. Phys.* **102**, 1133 (2001).
- [33] A. Dmitriev and V. Y. Kachorovskii, *Semiconductors* **42**, 934 (2008).
- [34] A. P. Dmitriev and V. Y. Kachorovskii, *Phys. Rev. B* **77**, 193308 (2008).
- [35] P. Drude, *Ann. Phys.* **306**, 566 (1900).
- [36] H. Spohn, *Rev. Mod. Phys.* **52**, 569 (1980).
- [37] A. Nota, C. Saffirio, and S. Simonella, in *Annales de l'Institut Henri Poincaré, Probabilités et Statistiques* (Institut Henri Poincaré, Paris, 2022), Vol. 58, pp. 1228–1243.
- [38] W. Götze and E. Leutheuser, *Z. Phys. B* **45**, 85 (1981).
- [39] M. P. Allen and D. J. Tildesley, *Computer Simulation of Liquids, 2nd ed.* (Oxford University Press, Oxford, 2017).
- [40] A. Kuzmany and H. Spohn, *Phys. Rev. E* **57**, 5544 (1998).
- [41] N. H. Siboni, J. Schluck, K. Pierz, H. W. Schumacher, D. Kazazis, J. Horbach, and T. Heinzl, *Phys. Rev. Lett.* **120**, 056601 (2018).
- [42] G. M. Gusev, P. Basmaji, Z. D. Kvon, L. V. Litvin, Y. Nastaushv, and A. I. Toropov, *J. Phys.: Condens. Matter* **6**, 73 (1994).

- [43] N. M. Sotomayor, G. M. Gusev, J. R. Leite, A. A. Bykov, A. K. Kalagin, V. M. Kudryashev, and A. I. Toropov, *Phys. Rev. B* **70**, 235326 (2004).
- [44] L. Bockhorn, I. V. Gornyi, D. Schuh, C. Reichl, W. Wegscheider, and R. J. Haug, *Phys. Rev. B* **90**, 165434 (2014).
- [45] T. Ando, *J. Phys. Soc. Jpn.* **37**, 1044 (1974).
- [46] T. Heinzl, *Mesoscopic Electronics in Solid State Nanostructures* (John Wiley & Sons, Hoboken, NJ, 2008).
- [47] J. Schluck, M. Hund, T. Heckenthaler, T. Heinzl, N. H. Siboni, J. Horbach, K. Pierz, H. W. Schumacher, D. Kazazis, U. Gennser, and D. Maily, *Phys. Rev. B* **97**, 115301 (2018).
- [48] I. V. Gornyi and A. D. Mirlin, *Phys. Rev. B* **69**, 045313 (2004).
- [49] T. J. Thornton, M. L. Roukes, A. Scherer, and B. P. Van de Gaag, *Phys. Rev. Lett.* **63**, 2128 (1989).
- [50] A. D. Mirlin, D. G. Polyakov, F. Evers, and P. Wölfle, *Phys. Rev. Lett.* **87**, 126805 (2001).
- [51] A. T. Hatke, M. A. Zudov, L. N. Pfeiffer, and K. W. West, *Phys. Rev. B* **83**, 121301(R) (2011).
- [52] L. Bockhorn, P. Barthold, D. Schuh, W. Wegscheider, and R. J. Haug, *Phys. Rev. B* **83**, 113301 (2011).
- [53] L. Bockhorn, A. Velieva, S. Hakim, T. Wagner, E. P. Rugeramigabo, D. Schuh, C. Reichl, W. Wegscheider, and R. J. Haug, *Appl. Phys. Lett.* **108**, 092103 (2016).
- [54] R. G. Mani, A. Kriisa, and W. Wegscheider, *Sci. Rep.* **3**, 2747 (2013).
- [55] A. T. Hatke, M. A. Zudov, J. L. Reno, L. N. Pfeiffer, and K. W. West, *Phys. Rev. B* **85**, 081304(R) (2012).
- [56] B. A. Sanvee, R. Lohmann, and J. Horbach, *Phys. Rev. E* **106**, 024104 (2022).